

A stable wavelength-tunable triggered source of single photons and cascaded photon pairs at the telecom C-band

Katharina D. Zeuner, Matthias Paul, Thomas Lettner, Carl Reuterskiöld Hedlund, Lucas Schweickert, Stephan Steinhauer, Lily Yang, Julien Zichi, Mattias Hammar, Klaus D. Jöns, and Val Zwiller

Citation: *Appl. Phys. Lett.* **112**, 173102 (2018); doi: 10.1063/1.5021483

View online: <https://doi.org/10.1063/1.5021483>

View Table of Contents: <http://aip.scitation.org/toc/apl/112/17>

Published by the [American Institute of Physics](#)

Articles you may be interested in

[Mid-infrared GaSb-based resonant tunneling diode photodetectors for gas sensing applications](#)

Applied Physics Letters **112**, 161107 (2018); 10.1063/1.5025531

[Demonstration of high mobility and quantum transport in modulation-doped \$\beta\$ -\(Al_xGa_{1-x}\)₂O₃/Ga₂O₃ heterostructures](#)

Applied Physics Letters **112**, 173502 (2018); 10.1063/1.5025704

[Abnormal growth kinetics of h-BN epitaxial monolayer on Ru\(0001\) enhanced by subsurface Ar species](#)

Applied Physics Letters **112**, 171601 (2018); 10.1063/1.5021326

[Simple 2.5 GHz time-bin quantum key distribution](#)

Applied Physics Letters **112**, 171108 (2018); 10.1063/1.5027030

[Full-color tuning in binary polymer:perovskite nanocrystals organic-inorganic hybrid blends](#)

Applied Physics Letters **112**, 171904 (2018); 10.1063/1.5020201

[Ionic conduction in sodium azide under high pressure: Experimental and theoretical approaches](#)

Applied Physics Letters **112**, 173903 (2018); 10.1063/1.5028468

PHYSICS TODAY

WHITEPAPERS

MANAGER'S GUIDE

Accelerate R&D with
Multiphysics Simulation

READ NOW

PRESENTED BY

 COMSOL

A stable wavelength-tunable triggered source of single photons and cascaded photon pairs at the telecom C-band

Katharina D. Zeuner,¹ Matthias Paul,¹ Thomas Lettner,¹ Carl Reuterskiöld Hedlund,² Lucas Schweickert,¹ Stephan Steinhauer,¹ Lily Yang,¹ Julien Zichi,¹ Mattias Hammar,² Klaus D. Jöns,^{1(a)} and Val Zwiller¹

¹Department of Applied Physics, Royal Institute of Technology, Albanova University Centre, Roslagstullsbacken 21, 106 91 Stockholm, Sweden

²Department of Electronics, Royal Institute of Technology, Electrum 229, 164 40 Kista, Sweden

(Received 4 January 2018; accepted 22 March 2018; published online 25 April 2018)

The implementation of fiber-based long-range quantum communication requires tunable sources of single photons at the telecom C-band. Stable and easy-to-implement wavelength-tunability of individual sources is crucial to (i) bring remote sources into resonance, (ii) define a wavelength standard, and (iii) ensure scalability to operate a quantum repeater. So far, the most promising sources for true, telecom single photons are semiconductor quantum dots, due to their ability to deterministically and reliably emit single and entangled photons. However, the required wavelength-tunability is hard to attain. Here, we show a stable wavelength-tunable quantum light source by integrating strain-released InAs quantum dots on piezoelectric substrates. We present triggered single-photon emission at 1.55 μm with a multi-photon emission probability as low as 0.097, as well as photon pair emission from the radiative biexciton–exciton cascade. We achieve a tuning range of 0.25 nm which will allow us to spectrally overlap remote quantum dots or tuning distant quantum dots into resonance with quantum memories. This opens up realistic avenues for the implementation of photonic quantum information processing applications at telecom wavelengths. © 2018 Author(s). All article content, except where otherwise noted, is licensed under a Creative Commons Attribution (CC BY) license (<http://creativecommons.org/licenses/by/4.0/>).

<https://doi.org/10.1063/1.5021483>

Creating single photons on-demand is one of the essential requirements to connect remote nodes of a quantum network using quantum repeaters. In the past few years, semiconductor quantum dots (QDs) have proven to be excellent sources of on-demand single,^{1–3} indistinguishable photons^{4–6} and entangled photon pairs.⁷ These photons will play a crucial role as flying qubits in quantum communication and quantum information processing. QDs are scalable and straightforward to integrate with advanced nanofabrication. They can be electrically driven with high excitation rates⁸ and enhanced extraction efficiency.⁹ Furthermore, QDs possess a tailorable emission wavelength based on a wide range of available semiconductor materials and growth methods. In order to enable long-range optical communication, emission wavelengths within the telecommunication C-band (1530–1565 nm) are required, due to the absorption minimum in the glass fiber material at these wavelengths. These emission wavelengths are long compared to the well-studied emission of typical InAs/GaAs QDs and have, previously, only been realized in the InAs/InP material system.^{10–12} However, the latter material system is brittle, distributed Bragg mirrors are hard to realize, and the optical quality of the QDs is lagging behind compared to QDs on GaAs substrates. Very recently, the first C-band QDs in the InGaAs/GaAs material system were fabricated¹³ by carefully engineering the interface between the substrate and the QD layer, thus providing a surface with a reduced lattice mismatch.

The application of such a metamorphic buffer layer (MMBL)^{14,15} allows emission of single and entangled photon pairs at a wavelength of 1.55 μm .¹⁶ However, based on the stochastic growth process of self-assembled QDs, there is a distribution in size and shape within a QD ensemble, as well as fluctuations in the QD's electrical environment, leading to a distribution of the emission wavelength. Hence, spectrally overlapping photons from different QDs require either the inefficient process of searching for nearly identical QDs or applying emission energy tuning mechanisms. To facilitate this, several tuning mechanisms for semiconductor QDs have been studied in the recent past, i.e. tuning via temperature, lateral and vertical electric^{17–19} or magnetic²⁰ fields, as well as strain.^{21,22} Tuning the QD emission wavelength via temperature, however, increases the interaction of charge carriers with phonons, thereby degrading the single-photon purity and introducing additional spectral broadening.²³ Using electric fields possesses the disadvantage of separating electrons and holes from each other, leading to decreased emission rates. Finally, tuning via magnetic fields requires the integration of large magnets into the setup, making it unfeasible for an application. In contrast, strain tuning offers a cheap and easily integrable method that allows the control of the optical properties of the QDs. Recently, complex piezo-tuning devices have been realized, which allow the simultaneous tuning of QD emission energy and fine structure splitting (FSS), thus enabling the generation of energy-tunable entangled photon pairs.^{24,25} The described tuning techniques to create a QD device showing tunable

^{a)}Author to whom correspondence should be addressed: klausj@kth.se

single-photon emission at $1.55\ \mu\text{m}$ have not yet been realized: until now, only the effect of uniaxial stress on the FSS of InAs/GaAs QDs at the telecom O-band has been reported.²⁶ In particular, piezoelectric strain tuning has not been employed yet for QDs emitting at the telecom C-band, due to the challenging InP material system rendering integration impossible. Here, we report on piezoelectric strain tuning of the emission wavelength from a mechanically thinned sample with InGaAs/GaAs QDs emitting at the telecom C-band. The sample is fabricated in a commercial AIX-200 horizontal flow reactor at a pressure of 100 mbar on exactly oriented (100), Si-doped GaAs substrates. As precursors, we used TMGa, TMI_n, TMAI, and AsH₃. In a first step, we deposited a distributed Bragg reflector (DBR) consisting of 20 alternating pairs of AlAs/GaAs with nominal thicknesses of 150 nm and 100 nm, respectively, followed by an InGaAs layer of 1150 nm and an additional 280 nm thick InGaAs capping layer. This structure forms a 3λ cavity between DBR and the semiconductor-air interface. We optimized the cavity for a wavelength of 1550 nm. The single layer of InAs QDs is deposited on top of the metamorphic InGaAs layer. This position lies in an anti-node of the standing electric wave and, thus, leads to an increase in the coupling between excitonic states and the resonator. For the metamorphic InGaAs layer, we increased the Indium flux during the growth time, i.e., the Indium concentration in the buffer increases with the thickness, decreasing the InAs/InGaAs lattice mismatch. More details on the sample growth are given in Ref. 13. For stable and reversible energy tuning of our quantum dot emission, we integrate the sample on a gold coated PMN-PT piezoelectric actuator (TRS technologies, thickness of $200\ \mu\text{m}$, $\langle 001 \rangle$ orientation). In order to increase the tuning range, the quantum dot sample is mechanically thinned using diamond-based abrasive films. The mechanical lapping of the sample allows for the integration of samples with arbitrary epitaxial layer structures (including DBRs), in contrast to chemical etching methods using a sacrificial layer.^{27,28} The sample surface is glued to the end of a brass rod with removable wax to apply uniform pressure during the lapping process. The sample thickness is monitored using a plunger dial. After the desired thickness of approximately $50\ \mu\text{m}$ is reached, the sample is released from the polishing rod in an acetone bath. Afterwards, the sample is carefully sieved from the bath using soft membrane tissue. We developed a reliable transfer method exploiting electrostatic forces to pick and place the thinned sample on the prepared piezo. By using a bendable soft tip to which the sample attaches during transfer, we are able to handle samples with thicknesses down to $15\ \mu\text{m}$. The bendable transfer tip is electrically charged via the triboelectric effect and then brought in soft contact with the sample top surface. The sample is picked up via weak Van der Waals forces. Once picked up, the sample can be transferred onto the glue-covered surface of the piezoelectric actuator. As a glue we use cryogenic epoxy (Stycast, two component resin) to achieve a rigid connection between the sample and the piezo actuator as well as good thermal contact. We attach the piezoelectric actuator only in one of its corners to the copper sample mount with conductive silver paste since a larger glued area would restrict the movement of the piezo actuator. Unrestricted

contraction and expansion of the piezo ensure a maximum transfer of stress to the sample. A schematic of the sample design is shown in Fig. 1(a) illustrating from bottom to top: gold-coated piezo (for electrical contacting), DBR layers, MMBL with QDs on top, and the capping layer. Between the top and the bottom of the piezoelectric element, a voltage can be applied to strain the sample. The sample is cooled to about 10 K in a closed-cycle cryostat. In our confocal microscopy setup, the sample is excited through a microscope objective (0.85 NA, $100\times$ magnification). A stack of three piezoelectric positioners is used in order to precisely position the QD under investigation underneath the microscope objective and furthermore allows us to scan the sample during excitation. We perform above-band excitation of the QD by using either a narrowband continuous wave (cw) laser at 795 nm or a tunable pulsed laser with a repetition rate of 80 MHz and a pulse duration of 2 ps. The QD photons are coupled into a single-mode fiber and are then sent either to a spectrometer that is equipped with an InGaAs array for spectral analysis or to superconducting single-photon detectors (SSPDs) optimized for telecom wavelengths to perform correlation measurements. For the spectral filtering during the correlation measurements, we use tunable fiber-based filters with a 3 dB-bandwidth of 0.8 nm. We take scanning electron microscopy (SEM) images of the cleaved facet of the non-thinned sample to investigate layer thicknesses as presented in Fig. 1(b). From bottom to top, the uppermost layers of the DBR, the metamorphic buffer, the QD layer, and the capping layer are visible. For the thickness of the metamorphic buffer, we measure $1.15\ \mu\text{m}$, and the capping layer thickness

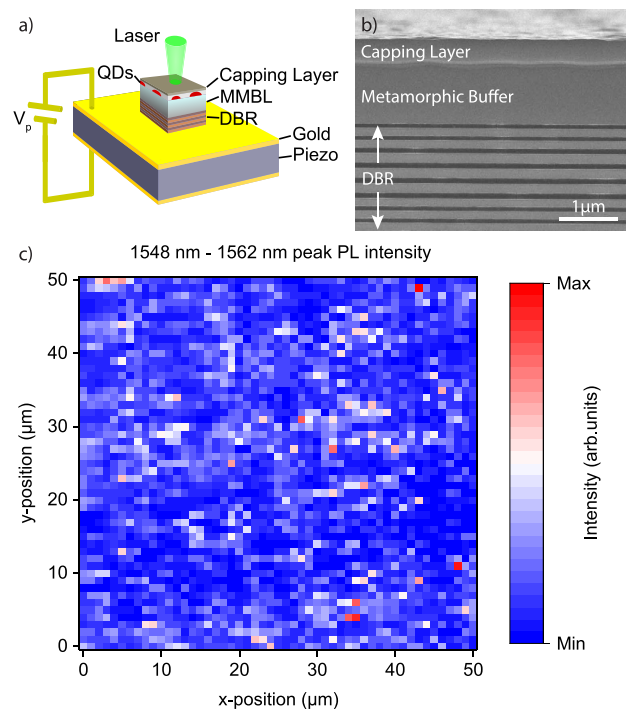


FIG. 1. (a) Sample schematic: the mechanically thinned sample glued to a piezoelectric element which is connected to a PCB via compression bonding. For simplicity, the remaining substrate is not depicted. (b) SEM image of a cleaved facet of the non-thinned sample. From bottom to top: top DBR layers, metamorphic buffer layer, QDs, and capping layer. (c) Photoluminescence map of the sample in a $50 \times 50\ \mu\text{m}$ range. Displayed is the PL peak intensity in a wavelength range of 1548 to 1562 nm.

is 250–300 nm. We observe undulations in the thickness of the MMBL, which is consistent with the findings in Ref. 13. These undulations are also observed for the capping layer thickness. For further characterization, we record photoluminescence (PL) maps by scanning the sample in $1\ \mu\text{m}$ steps in an area of $50 \times 50\ \mu\text{m}$ during above-band cw excitation. At each position, we take a spectrum with an integration time of 2 s in a spectral range of 1548 nm–1562 nm. The results are presented in Fig. 1(c), where the peak intensity is plotted over the position of the piezo actuators with a read-out accuracy of 500 nm. The PL map allows us to assess not only the density of optically active QDs but also their distribution on the sample. We infer a QD density on the order of $10^7\ \text{cm}^{-2}$. Assuming a spot diameter on the sample of $1\ \mu\text{m}$, we find on average only one QD in the excitation spot, which is ideal for single QD spectroscopy. Moreover, from the data collected for the PL map, we can conclude an ensemble bandwidth of 12 meV.

In Fig. 2(a), we present the spectrum of QD 1 with emission at the telecom C-band. The spectrum consists of an exciton (X), a trion (T), and a biexciton (XX) transition. The three different s-shell states were identified via power and polarization dependent measurements. Below the spectrum, we present a tuning map, displaying the emission wavelength as a function of the applied voltage to the piezoelectric

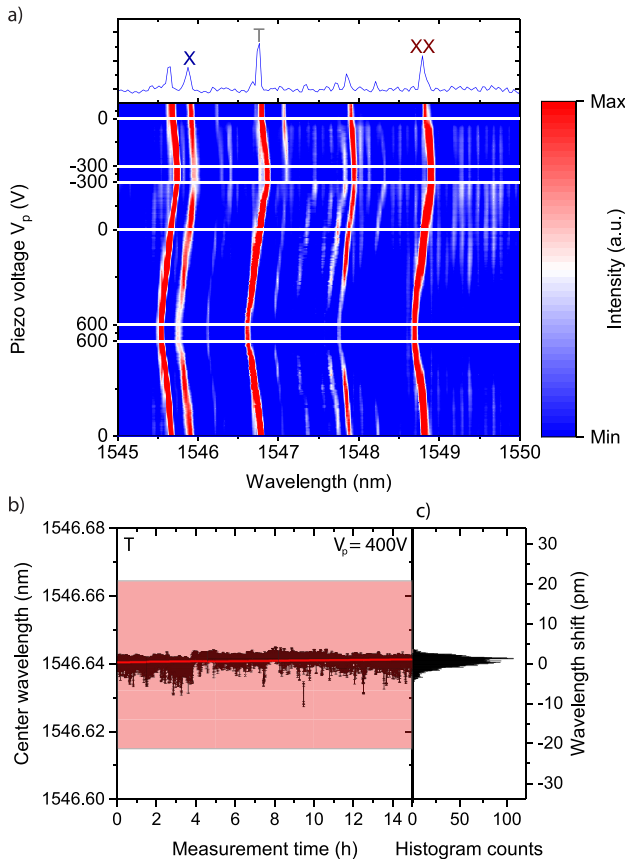


FIG. 2. (a) Top image: PL spectrum of QD 1 at 0 V, denoted are exciton (X), trion (T), and biexciton (XX) states, and the intensity is plotted in arbitrary units. Bottom image: QD emission as a function of applied voltage to the piezo in an overall range of 900 V. (b) Center wavelength of the T line for an applied voltage of +400 V plotted over a measurement duration of 15 h. The red area spans over the bandwidth corresponding to the CCD resolution. Marked with a red line is a fit to the data. (c) Histogram of wavelength shifts.

actuator. Positive (negative) voltage corresponds to in-plane compression (expansion) of the positively poled piezo actuator. We operate the piezo in a voltage range of +600 V to –300 V to ensure repeatability and reproducibility of the strain tuning. The voltage was changed in 1 V steps, and for every step, we take a spectrum with an integration time of 10 s. The starting point is the emission of the sample at 0 V, and then, the applied voltage is increased to +600 V and then held there for 1000 s, while continuously recording spectra. Following this, the applied voltage is reduced to –300 V and then again ramped to 0 V, with stops for 1000 s at –300 V and 0 V, again marked by vertical lines. Tuning towards higher positive voltages corresponds to a blue-shift of the emission, whereas tuning towards lower voltages leads to a red-shift of the emission wavelengths. We extract the tuning range of the emission wavelength from fits to the spectra. We find a tuning range of 0.25 nm, which corresponds to $0.28\ \text{pm V}^{-1}$, which allows extremely precise tuning of quantum dot emission. Over the entire tuning range, the linewidth of the emission lines remains constant, and typical linewidths are on the order of $20\ \mu\text{eV}$ (resolution limited in our spectrometer). Furthermore, the observed wavelength shift is reversible and follows the same linear behavior for all lines under investigation within our setup resolution. While a broad tuning range is desired in order to be able to reach a target wavelength with a large number of QDs, the long-term stability of the emission once tuned to the target wavelength is of equal importance for reliable operation. An investigation of the emission wavelength of the trion-line over a measurement period of 15 h for an applied voltage of 400 V is shown in Fig. 2(b). The individual center wavelength of each spectrum is obtained via fits to the data, as the change in wavelength over time is clearly below the resolution limit of the spectrometer. We mark the spectral bandwidth corresponding to the CCD resolution of $25\ \mu\text{eV}$, to further illustrate the long-term stability of our tunable source. A linear fit to the data is shown in Fig. 2(b), and we find a slope of zero within the fit error. This order of stability enables a long-term overlap of QD photons with respect to a specific resonance.²⁹ Furthermore, we plot the shifts in wavelength compared to the central wavelength according to the linear fit in a histogram in Fig. 2(c). From this, we can infer a wavelength stability of $(2.43 \pm 0.07)\ \text{pm}/15\ \text{h}$.

Finally, we investigate photon statistics properties of the telecom C-band quantum dot emission. A second-order auto-correlation measurement is performed to analyze the multi-photon emission probability. For this, the QD under investigation (QD 2) is excited with 2 ps pulses at 780 nm and the photons of the emission line [Fig. 3(a), inset] are filtered with a tunable fiber-based filter and then sent onto a 50:50 beam splitter. A start–stop measurement is carried out with two SSPDs, and the correlation histogram is recorded and displayed in Fig. 3(a). Strong suppression of the peak at zero time delay is apparent, which corresponds to a low probability of multi-photon emission. The contribution of multi-photon events is calculated via a fit to the data according to Ref. 30 and gives a value of 0.097 ± 0.045 . The fit takes the population dynamics of the quantum two-level system into account and is able to reproduce the dip observed at zero time delay. Furthermore, we perform a cross-correlation measurement of

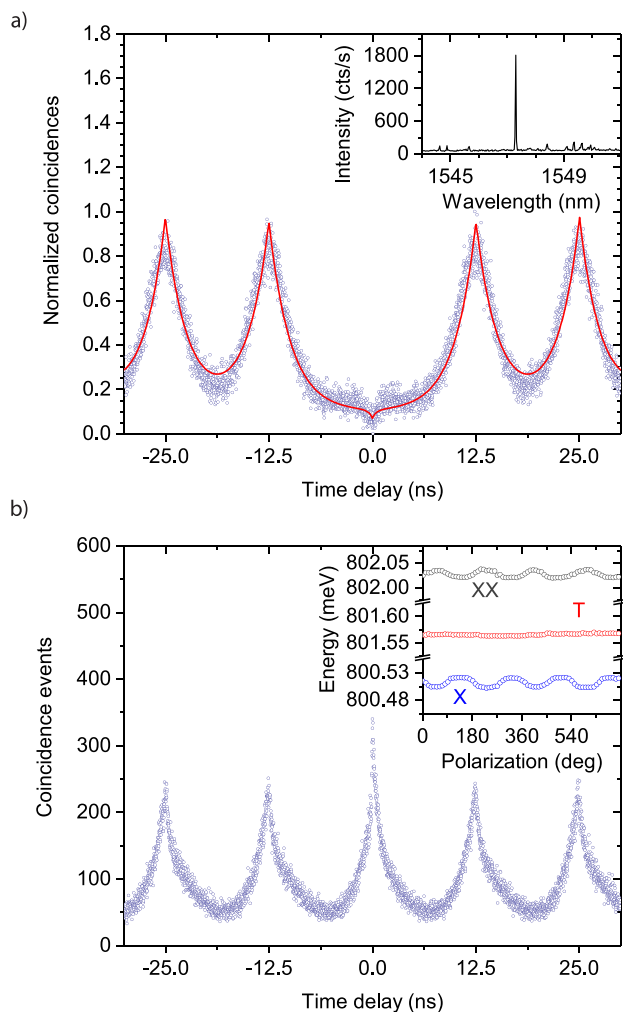


FIG. 3. (a) Second-order auto-correlation function measured under pulsed excitation of QD 2; the spectrum is shown in the inset. (b) Cross-correlation function of the biexciton (XX) and the exciton (X) of QD 1. Inset: result of the polarization-dependent measurement of QD 1, shown for X, T, and XX.

X and XX of QD 1 under pulsed excitation. The emission of QD 1 is split with a 50:50 beam splitter, and then, a fiber-based filter in each arm is set to either the X (1546.9 nm) or the XX wavelength (1549.9 nm). Subsequently, a start–stop measurement between the XX and X photons is performed. The existence of an XX–X–cascade is clearly visible in Fig. 3(b). Once the XX state decayed, the probability of the emission of an X photon increases, leading to the observed bunching peak for zero time delay, thus confirming the existence of a radiative cascade. We extract an exciton lifetime of (1.29 ± 0.04) ns, which is a typical lifetime for QDs of this sample. Cascaded emission of photon pairs via the radiative cascade results in polarization entangled photon pairs.³¹ However, the QD under investigation exhibits a fine structure-splitting of $34.8 \mu\text{eV}$, as shown in the inset of Fig. 3(b), leading to a fast time-evolving entangled state.³²

In conclusion, we have demonstrated precise emission energy tuning of single and cascaded photons at 1550 nm with high precision, using a piezoelectric substrate. We achieved a tuning range of 0.25 nm, which is enough to tune QDs in a spectral distance of 0.5 nm into resonance and, thus, demonstrates the potential of strain tuning in telecom QDs. Furthermore, we show that the targeted wavelength

after tuning is stable, which allows us to perform long-term experiments with this type of device. The demonstrated wavelength tunability will be of crucial importance to spectrally overlap remote QDs for entanglement swapping operations and tuning QDs into resonance with quantum memories.

The authors thank Raffaele Gallo for contributions to sample growth. The Quantum Nano Photonics Group at KTH acknowledges the continuous support of the company APE on their picoEmerald system. K.D.Z. gratefully acknowledges funding by the Dr. Isolde Dietrich Foundation. K.D.J. acknowledges funding from the MARIE SKŁODOWSKA-CURIE Individual Fellowship under REA Grant Agreement No. 661416 (SiPhoN). V.Z. acknowledges funding by the European Research Council under the Grant Agreement No. 307687 (NaQuOp) and the Swedish Research Council under Grant Agreement No. 638-2013-7152. Financial support was also provided by the Linnaeus Center in Advanced Optics and Photonics (Adopt). This project was co-funded by Vinnova and FP7 (GROWTH 291795).

¹Y.-M. He, Y. He, Y.-J. Wei, D. Wu, M. Atatüre, C. Schneider, S. Höfling, M. Kamp, C.-Y. Lu, and J.-W. Pan, *Nat. Nanotechnol.* **8**, 213 (2013).

²P. Senellart, G. Solomon, and A. White, *Nat. Nanotechnol.* **12**, 1026 (2017).

³L. Schweickert, K. D. Jöns, K. D. Zeuner, S. Filipe, H. Huang, T. Lettner, M. Reindl, J. Zichi, R. Trotta, A. Rastelli, and V. Zwiller, *Appl. Phys. Lett.* **112**, 093106 (2018).

⁴C. Santori, D. Fattal, J. Vučković, G. S. Solomon, and Y. Yamamoto, *Nature* **419**, 594 (2002).

⁵N. Somaschi, V. Giesz, L. De Santis, J. C. Loredó, M. P. Almeida, G. Hornecker, S. L. Portalupi, T. Grange, C. Anton, J. Demory, C. Gomez, I. Sagnes, N. D. L. Kimura, A. Lemaitre, A. Auffeves, A. G. White, L. Lanco, and P. Senellart, *Nat. Photonics* **10**, 340 (2016).

⁶X. Ding, Y. He, Z. C. Duan, N. Gregersen, M. C. Chen, S. Unsleber, S. Maier, C. Schneider, M. Kamp, S. Höfling, C. Y. Lu, and J. W. Pan, *Phys. Rev. Lett.* **116**, 020401 (2016).

⁷M. Müller, S. Bounouar, K. D. Jöns, M. Glässl, and P. Michler, *Nat. Photonics* **8**, 224 (2014).

⁸F. Hargart, C. A. Kessler, T. Schwarzback, E. Koroknay, S. Weidenfeld, M. Jetter, and P. Michler, *Appl. Phys. Lett.* **102**, 011126 (2013).

⁹T. Heindel, C. Schneider, M. Lerner, S. H. Kwon, T. Braun, S. Reitzenstein, S. Höfling, M. Kamp, and A. Forchel, *Appl. Phys. Lett.* **96**, 011107 (2010).

¹⁰T. Miyazawa, K. Takemoto, Y. Sakuma, S. Hirose, T. Usuki, N. Yokoyama, M. Takatsu, and Y. Arakawa, *Jpn. J. Appl. Phys., Part 2* **44**, L620 (2005).

¹¹M. D. Birowosuto, H. Sumikura, S. Matsuo, H. Taniyama, P. J. van Veldhoven, R. Nötzel, and M. Notomi, *Sci. Rep.* **2**, 321 (2012).

¹²M. Benyoucef, M. Yacob, J. P. Reithmaier, J. Kettler, and P. Michler, *Appl. Phys. Lett.* **103**, 162101 (2013).

¹³M. Paul, F. Olbrich, J. Höschele, S. Schreier, J. Kettler, S. L. Portalupi, M. Jetter, and P. Michler, *Appl. Phys. Lett.* **111**, 033102 (2017).

¹⁴N. Ledentsov, A. Kovsh, A. Zhukov, N. Maleev, S. Mikhlin, A. Vasil'ev, E. Semenova, M. Maximov, Y. Shernyakov, N. Kryzhanovskaya, V. Ustinov, and D. Bimberg, *Electron. Lett.* **39**, 1126 (2003).

¹⁵E. S. Semenova, R. Hostein, G. Patriarche, O. Mauguin, L. Largeau, I. Robert-Philip, A. Beveratos, and A. Lemaitre, *J. Appl. Phys.* **103**, 103533 (2008).

¹⁶F. Olbrich, J. Höschele, M. Müller, J. Kettler, S. Luca Portalupi, M. Paul, M. Jetter, and P. Michler, *Appl. Phys. Lett.* **111**, 133106 (2017).

¹⁷K. Kowalik, O. Krebs, A. Lemaitre, S. Laurent, P. Senellart, P. Voisin, and J. A. Gaj, *Appl. Phys. Lett.* **86**, 041907 (2005).

¹⁸B. D. Gerardot, S. Seidl, P. A. Dalgarno, R. J. Warburton, D. Granados, J. M. Garcia, K. Kowalik, O. Krebs, A. Badolato, P. M. Petroff, B. D. Gerardot, S. Seidl, P. A. Dalgarno, and R. J. Warburton, *Appl. Phys. Lett.* **90**, 041101 (2007).

¹⁹S. Marcet, K. Ohtani, and H. Ohno, *Appl. Phys. Lett.* **96**, 101117 (2010).

- ²⁰M. Bayer, G. Ortner, O. Stern, A. Kuther, A. A. Gorbunov, A. Forchel, P. Hawrylak, S. Fafard, K. Hinzer, T. L. Reinecke, S. N. Walck, J. P. Reithmaier, F. Klopff, and F. Schäfer, *Phys. Rev. B* **65**, 195315 (2002).
- ²¹S. Seidl, M. Kroner, A. Högele, K. Karrai, R. J. Warburton, A. Badolato, and P. M. Petroff, *Appl. Phys. Lett.* **88**, 203113 (2006).
- ²²K. D. Jöns, R. Hafenbrak, R. Singh, F. Ding, J. D. Plumhof, A. Rastelli, O. G. Schmidt, G. Bester, and P. Michler, *Phys. Rev. Lett.* **107**, 217402 (2011).
- ²³S. Varoutsis, S. Laurent, P. Kramper, A. Lemaître, I. Sagnes, I. Robert-Philip, and I. Abram, *Phys. Rev. B* **72**, 041303 (2005).
- ²⁴R. Trotta, J. Martín-Sánchez, J. S. Wildmann, G. Piredda, M. Reindl, C. Schimpf, E. Zallo, S. Stroj, J. Edlinger, and A. Rastelli, *Nat. Commun.* **7**, 10375 (2016).
- ²⁵Y. Chen, J. Zhang, M. Zopf, K. Jung, Y. Zhang, R. Keil, F. Ding, and O. G. Schmidt, *Nat. Commun.* **7**, 10387 (2016).
- ²⁶L. Sapienza, R. N. Malein, C. E. Kuklewicz, P. E. Kremer, K. Srinivasan, A. Griffiths, E. Clarke, M. Gong, R. J. Warburton, and B. D. Gerardot, *Phys. Rev. B* **88**, 155330 (2013).
- ²⁷T. Zander, A. Herklotz, S. Kiravittaya, M. Benyoucef, F. Ding, P. Atkinson, S. Kumar, J. D. Plumhof, K. Dörr, A. Rastelli, and O. G. Schmidt, *Opt. Express* **17**, 22452 (2009).
- ²⁸A. Rastelli, F. Ding, J. D. Plumhof, S. Kumar, R. Trotta, C. Deneke, A. Malachias, P. Atkinson, E. Zallo, T. Zander, A. Herklotz, R. Singh, V. Krápek, J. R. Schröter, S. Kiravittaya, M. Benyoucef, R. Hafenbrak, K. D. Jöns, D. J. Thurmer, D. Grimm, G. Bester, K. Dörr, P. Michler, and O. G. Schmidt, *Phys. Status Solidi (B) Basic Res.* **249**, 687 (2012).
- ²⁹J. S. Wildmann, R. Trotta, J. Martín-Sánchez, E. Zallo, M. O'Steen, O. G. Schmidt, and A. Rastelli, *Phys. Rev. B* **92**, 235306 (2015).
- ³⁰H. Nakajima, H. Kumano, H. Iijima, and I. Suemune, *Appl. Phys. Lett.* **101**, 161107 (2012).
- ³¹O. Benson, C. Santori, M. Pelton, and Y. Yamamoto, *Phys. Rev. Lett.* **84**, 2513 (2000).
- ³²M. Ward, M. Dean, R. Stevenson, A. Bennett, D. Ellis, K. Cooper, I. Farrer, C. Nicoll, D. Ritchie, and A. J. Shields, *Nat. Commun.* **5**, 3316 (2014).